



1 Numerical modeling of relative contribution of planetary waves to 2 the atmospheric circulation

3 Andrey V. Koval^{1,2}, Olga N. Toptunova², Maxim A. Motsakov², Ksenia A. Didenko^{1,2}, Tatiana S.
4 Ermakova^{1,2}, Nikolai M. Gavrilov¹, Eugene V. Rozanov³

5 ¹Atmospheric Physics Department, Saint-Petersburg State University, Saint Petersburg, 199034, Russia

6 ²Department of Meteorological Forecasts, Russian State Hydrometeorological University, 195196 Saint-Petersburg, Russia

7 ³Physikalisch-Meteorologisches Observatorium, Davos World Radiation Centre, Davos Dorf, 7260, Switzerland

8

9 *Correspondence to:* Eugene V. Rozanov (Eugene.Rozanov@pmodwrc.ch)

10 **Abstract.** Using the general circulation model of the middle and upper atmosphere (MUAM), a number of numerical
11 scenarios were implemented to study the impact of individual planetary waves (PWs) on the global atmospheric circulation,
12 including zonal wind, temperature, and residual meridional circulation. The calculations were performed for the winter
13 conditions of the Northern Hemisphere (January–February). The contribution to the formation of the dynamic and
14 temperature regimes of the middle and upper atmosphere made by equatorial Kelvin waves propagating to the east, as well
15 as atmospheric normal modes with periods from 4 to 16 days is shown. In particular, it is demonstrated that the impact of a
16 5-day PW and an ultrafast Kelvin wave can change the speed of circulation flows by up to 5% in the areas of their amplitude
17 maxima. The presented research results are important for a deeper understanding of the mechanisms of large-scale
18 atmospheric interactions. Despite the obviousness and simplicity of the problem, such work has not been carried out at the
19 moment.

20 **Keywords:** planetary waves, normal atmospheric modes, residual meridional circulation, numerical simulation, atmospheric
21 dynamics

22 1 Introduction

23 Planetary waves (PWs, known as Rossby waves) are large-scale variations in the hydrodynamic parameters of the
24 atmosphere (wind, temperature, density), which are formed due to the potential vorticity conservation. The horizontal
25 distribution of PWs is determined by the counteraction of the meridional gradient of the Coriolis force and the meridional
26 displacements of the jet streams. According to the classic theory (e.g., Holton, 1975), a number of waves fit along the
27 latitude circle, which is determined by the zonal wave number. The amplitudes of PWs increase due to a decrease in the
28 density of the atmosphere, when they propagate from their sources in the troposphere. In the middle and upper atmosphere
29 these disturbances become an important driver of the atmospheric circulation. One of the important features of planetary



30 waves is their active interaction with the mean flow causing transfer of energy and momentum. This feature was reflected in
31 the formulation of the generalized Eliassen Palm theorem (Eliassen and Palm, 1961). PWs can provide a significant
32 acceleration of the background flow in the middle atmosphere when dissipating. This acceleration is comparable to the
33 acceleration associated with gravity waves and atmospheric tides (e.g., Pogoreltsev, 1999).

34 Another important feature of PWs, which explains the need for their comprehensive study, is that they are a link
35 between different atmospheric layers and regions. The PWs can contribute to the signal propagation from the quasi-biennial
36 oscillation (QBO) of the equatorial zonal wind into the thermosphere (Koval et al., 2022) and from the equatorial region to
37 the extratropical region (Holton & Tan, 1980). The ability of PWs to be reflected downward at the heights of the lower
38 thermosphere, due to changes in vertical temperature gradients associated with solar activity cycle, can also have a
39 significant effect on the dynamic and temperature regimes of the middle atmosphere (Koval et al., 2018a).

40 According to the so-called “downward control principle” (Haynes et al., 1991), PWs are the main driving force of
41 meridional extratropical circulation (see also Holton et al., 1995). Due to its global nature, meridional circulation is
42 considered to be the most important mechanism of dynamic interaction between different layers and regions of the
43 atmosphere, affecting the transport of aerosol, atmospheric gases and, consequently, the composition of the atmosphere.
44 Changes in the meridional circulation can affect the ozone layer behavior. The state of the ozone layer has attracted
45 increased attention due to global ozone depletion (e.g., Newman et al, 2009). PWs are the main factor in the development of
46 sudden stratospheric warming (Schoeberl, 1978; Nath et al., 2016).

47 A lot of studies are currently dedicated to the PWs having different periods and zonal wavenumbers. For example,
48 numerical simulations of PWs influence were discussed in Liu et al. (2004); Chang et al. (2014); Wang et al. (2017); Forbes
49 et al. (2018; 2020); He et al. (2020) and many others. Ground based radar measurements were presented by Clark et al.
50 (2002); Jiang et al. (2008); Pancheva et al., (2008) and satellite measurements by Day et al. (2011); Forbes & Zhang (2017);
51 Pancheva et al., (2018); Merzlyakov et al. (2013), as well as processing of reanalysis data/weather forecasting system by
52 Sassi et al. (2011); Qin et al. (2021), etc.

53 In this paper we considered the relative contribution of various PW modes to the formation of the global
54 atmospheric circulation using the unique opportunity that numerical modeling gives us. In order to further understand the
55 nature of large-scale atmospheric dynamics, we carried out a number of numerical experiments to quantify the sensitivity of
56 the zonal wind and temperature fields, as well as meridional circulation components to the switching on/off sources of
57 various PW modes in the model. Despite the obviousness and simplicity of the problem, such work has not been carried out
58 at the moment.

59 2 Methodology

60 **The MUAM model.** Planetary waves are studied using the Middle and Upper Atmosphere Model (MUAM,
61 Pogoreltsev et al., 2007). MUAM is a three-dimensional nonlinear mechanistic model of the general atmospheric circulation



62 at heights from the surface to the F2 ionospheric layer (up to 300-400 km). This is one of the most promising and modern
63 models of atmospheric wave dynamics, which makes it possible study the processes in the middle and upper atmosphere, as
64 well as their interaction with lower levels (see, for example, Gavrilov et al., 2018; Ermakova et al., 2019; Koval et al., 2018a,
65 b; 2022; Medvedeva et al., 2019). One of the advantages of MUAM is that it allows us not only to analyze the amplitudes of
66 planetary waves, but also to associate them with various generating sources. The log-isobaric height $x = -H \ln(p/p_s)$ is used as
67 the vertical coordinate in MUAM, where p is the pressure in hPa, p_s is the surface pressure, and H is the pressure scale
68 height. The latitude and longitude spacing of horizontal grid of the model is $5.625^\circ \times 5^\circ$. A version of the model with 56
69 vertical levels is used, covering a vertical range from the Earth surface to about 300 km. The time integration step is 225 s.

70 The MUAM radiation module takes into account atmospheric net radiative heating due to solar and infrared
71 irradiance. The thermosphere includes parameterization of heating in the extreme ultraviolet band. Ion drag, molecular and
72 turbulent viscosity and thermal conductivity are included as well. The model provides the possibility of planetary waves'
73 excitation near the Earth's surface. The possibility of changing the albedo of the underlying surface is available. Weather
74 changes and cloudiness in the troposphere are not simulated. The MUAM uses three parametrizations of gravity waves with
75 different phase velocities, including orographic waves. For further description of the processes involved in the current
76 version of the model, please refer to Koval et al. (2022).

77 The main parameters simulated by the MUAM include 4-dimensional fields of the zonal, meridional and vertical
78 velocity components, geopotential height, and temperature with time step of 2 h. By the MUAM initialization, zonal mean
79 climatological distributions of the geopotential height and temperature are set with the lower boundary conditions at the
80 1000 hPa isobaric level. These distributions were obtained using the reanalysis MERRA-2 data (Gelaro, et al., 2017) and
81 averaged over 20 years (from 2000 to 2019) for January-February.

82 Since the MUAM does not reproduce tropospheric weather, the sources of the westward propagating PWs
83 (atmospheric normal modes, NMs) and the eastward PWs (Kelvin waves) in the MUAM are specified using additional terms
84 in the heat balance equation, having the form of time-dependent sinusoidal harmonics with zonal wavenumbers $m = 1$ and m
85 $= 2$, and periods matching to simulated PWs. To specify the latitudinal structure of the PW components, the corresponding
86 Hough functions obtained using the method described by Swarztrauber and Kasahara (1985) are used. PW periods are equal
87 to the resonant response of the atmosphere to the wave action at the lower boundary (Pogoreltsev, 1999). Westward
88 propagating NMs (1.1), (1.2), (1.3), and (2.1), (2.2) in the classification proposed by Longuet-Higgins (1968) are considered.
89 They have periods of about 5, 10, 16 days with a zonal number of 1, and about 4 and 7 days with a zonal number of 2. In
90 addition, eastward propagating ultrafast Kelvin wave (UFWK, having period of about 3.5 days, a zonal number of 1) are
91 studied.

92 **Residual meridional circulation.** A significant problem when considering meridional flows in the framework of
93 the classical Eulerian approach (i.e., with zonal averaging of meridional and vertical circulation flows) is that, in the
94 equations of dynamics, the wave sources of momentum and heat are compensated by advective flows of momentum and heat
95 (Charney and Drazin, 1961). This feature does not allow one to isolate and analyze the wave action on the mean flow. At the



96 same time, in the continuity equation for long-lived gas components, there is a compensation of wave and mean flows. Thus,
97 the use of the Eulerian mean meridional circulation is inefficient for calculating mass transfer and long-lived gas species. A
98 thorough analysis of this topic was made by Butchart (2014). In this study, the Transformed Eulerian Mean (TEM) approach,
99 introduced by Andrews and McIntyre (1976), was used to diagnose the impact of PW on the mean flow. The TEM approach
100 is based on consideration of the components of the mean residual meridional circulation (RMC), which is a superposition of
101 eddy and advective mean transport. Formulas for calculating the RMC components are presented, for example, by Koval et
102 al. (2022). The time-averaged RMC represents the net average movement of air masses and, therefore, in contrast to the
103 conventional mean Eulerian circulation, it approximates of the average advective movement of atmospheric species.

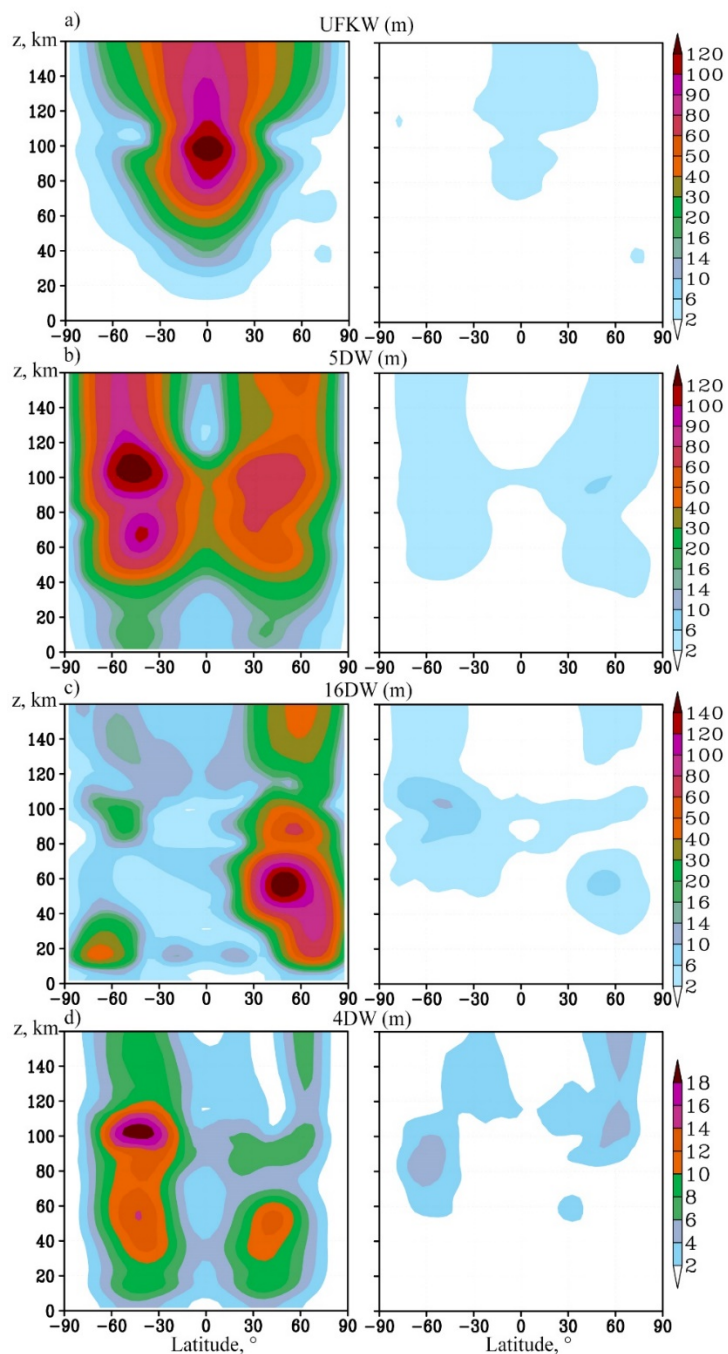
104 **Scenarios of model experiments.** A series of numerical experiments (model runs) was carried out for January-
105 February to identify the influence of various wave components on the variability of the global circulation and the RMC. The
106 scenarios of the model runs are presented in Table 1: a reference run of the model (#1) was carried out to calculate the
107 atmospheric circulation with the inclusion of all sources of the considered PWs, and other runs were performed with the
108 sources of individual waves turned off. Designations of 4DW, 5DW... mean PWs having periods of 4, 5 days and others.
109 UFKW means ultrafast Kelvin wave. The PW amplitudes were obtained using the longitude-time Fourier expansion into the
110 first 4 harmonics applied to the geopotential height fields. Next, an approximation was carried out using the least squares
111 method to the given oscillation periods.

112 **Table 1. Scenarios of model calculations, including different PWs.**

runs	4DW	5DW	7DW	10DW	16DW	UFKW
1	+	+	+	+	+	+
2	+	+	+	+	+	
3	+		+	+	+	+
4	+	+	+		+	+
5	+	+	+	+		+
6		+	+	+	+	+
7	+	+		+	+	+

114 3 Amplitudes of planetary waves

115 Fig. 1 shows the amplitudes of geopotential height variations due to the observing planetary waves for January-
116 February. The wave amplitude according to the results of the initial model simulation with the inclusion of sources of all
117 considered PWs (run #1) is presented on the left side. For comparison, the right panels show the amplitudes of these waves
118 for the model simulations with each wave source turned off (see scenarios in Table 1).



119

120

121

122

Figure 1. Amplitudes of variations of geopotential height (m) with the source of the respective PW in the MUAM been turned on (left panels) and off (right panels) for the following PW modes: a) Ultrafast Kelvin wave, b) 5-day PW, c) 16-day (all with a zonal wave number $m=1$); d) 4-day (with $m=2$). Note that the color scale is uneven.



123 The amplitude of eastward propagating UFKW (a period of about 3.5 days) is shown in Fig. 1a. Kelvin waves are
124 localized in the low latitude region unlike classic atmospheric NMs, the horizontal structure of which is caused primarily by
125 the action of the Coriolis force weakening hem near the equator. The UFKW is mainly excited by the tropospheric source
126 specified in the MUAM. Its generation by internal atmospheric interactions is relatively weak (compare the left and right
127 panels of Fig.1a). The westward propagating NMs, shown in Fig. 1b-d, have maxima in the middle latitudes of both
128 hemispheres. Waves with larger phase velocities (4-d and 5-d NMs) can propagate in both hemispheres (Fig. 1b and 1d),
129 while slower waves predominantly propagate through the eastward wind structures of the winter (in our case – the Northern)
130 hemisphere (Fig.11c). This is due to propagation barriers of these waves occurring when their phase velocity is less than the
131 westward zonal jet stream in the summer stratosphere and mesosphere (see, for example, Charney and Drazin, 1961).

132 Fig. 1 shows the deficiency of waves generation in the middle atmosphere inside the model, and the PW amplitudes
133 with the sources turned off (right panels) do not exceed a numerical noise level. An exception is the maximum amplitude of
134 16-day PW in the right Fig. 1c, which is formed at latitude near 60° S and altitude of about 100 km. When the tropospheric
135 source is turned off, this maximum of geopotential height reaches 15 m in the right panel of Fig. 1c, whereas it is about 24m
136 for the turned-on wave source (the left panel of Fig.1c). This reveals an interesting effect of 16-day PW generating by
137 internal atmospheric sources was discovered. The main source of the 16-day wave generating in the southern lower
138 thermosphere in the MUAM may be elucidated by the nonlinear interaction of the 5- and 4-day waves, whose amplitudes
139 have maxima in the same latitude-altitude region in the left panels of Fig. 1b and 1d. Therefore further study of this
140 phenomenon is required.

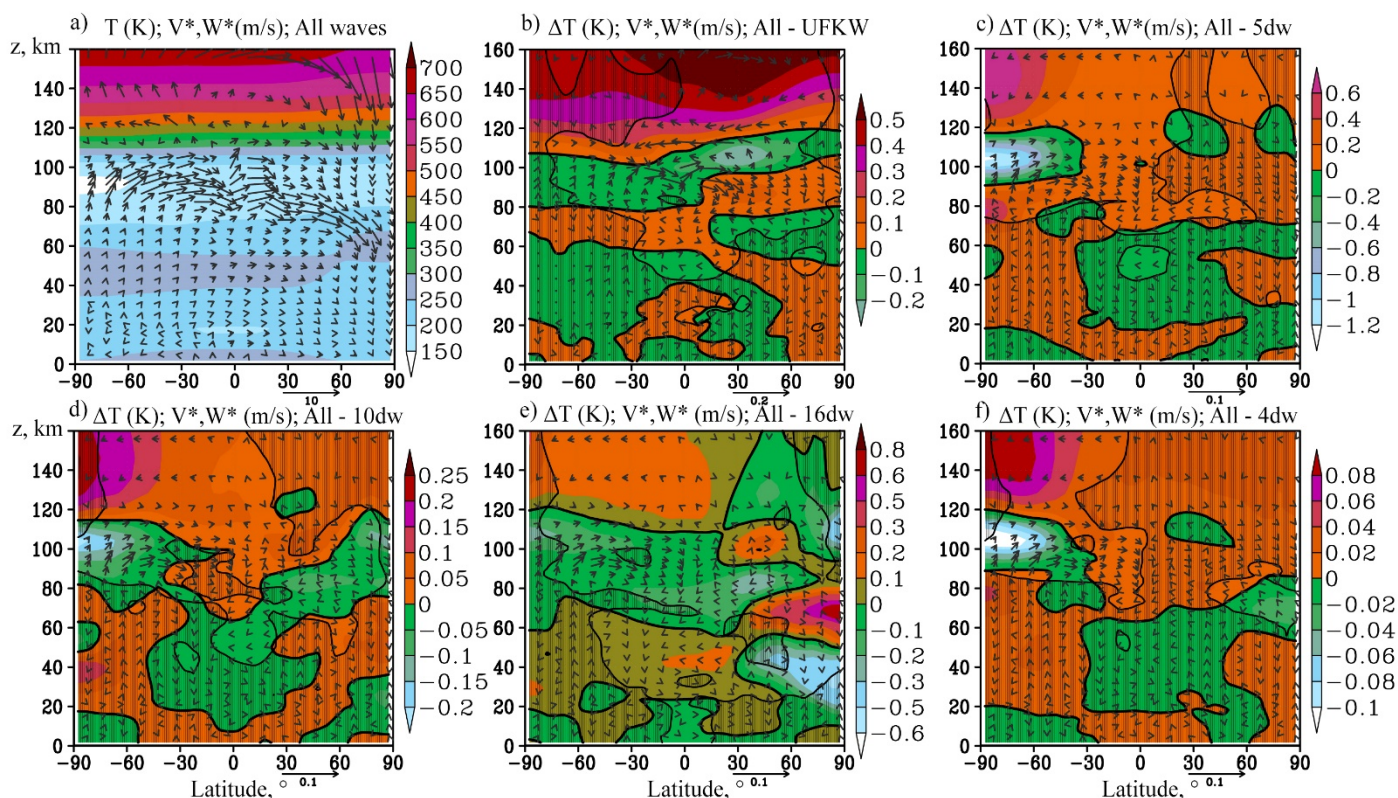
141 A detailed comparison of the MUAM-simulated PW amplitudes for January-February with satellite and radar
142 observations, also with reanalysis data was carried out. For example, the amplitudes of PWs in the geopotential field
143 calculated according to NCEP/NCAR reanalysis data at 10 and 30 hPa pressure levels were presented in the study by
144 Pancheva et al., (2008). The values of these amplitudes agree with our results. The calculated PW amplitudes in geopotential
145 height according to the MERRA-2 reanalysis data and averaged over the years used for the initialization of MUAM have
146 also similar value and structure to the simulated one's. Additionally, Yamazaki et al. (2021) presents the distributions of 4-
147 day PW amplitudes according to measurements of geopotential height using Aura satellite microwave sensing, the structure
148 of which corresponds to our calculations. Whereas, the presented values of the PW amplitudes may differ significantly,
149 which is primarily due to the fact that the data for individual specific days are presented in the specified article. The data
150 from the global numerical weather forecasting system (NOGAPS-ALPHA) is used by Sassi et al., (2012) to calculate
151 structures of geopotential height variations by atmospheric NMs. These structures are similar to our distributions. In
152 addition, the 5-day wave amplification in the southern mesosphere similar to the one demonstrated in the left Fig. 1a is
153 shown. For a more detailed analysis of the simulated PWs, in order to compare with the published data, the amplitudes of
154 temperature variations by PWs were also calculated. The simulated 5-day PW and UFKW in temperature field were
155 compared, in particular, with the wave amplitudes calculated from TIMED/SABER temperature data (Pancheva et al., 2010).
156 The amplitude values accordance (up to 6 K at the MLT height for January for 5-day PW at the mid-latitudes of both



157 hemispheres, for UFKW - at the equator) and the spatial distribution accordance of PW across latitudes were found.
158 Moreover, the simulated PW amplitudes correlate in magnitude and spatial distribution with the respective waves obtained in
159 a number of studies (Pancheva et al., 2008, 2009; Forbes et al., 2017; Pedatella & Forbes, 2009; Huang et al., 2017).

160 4 Relative PW contribution to the general atmospheric circulation

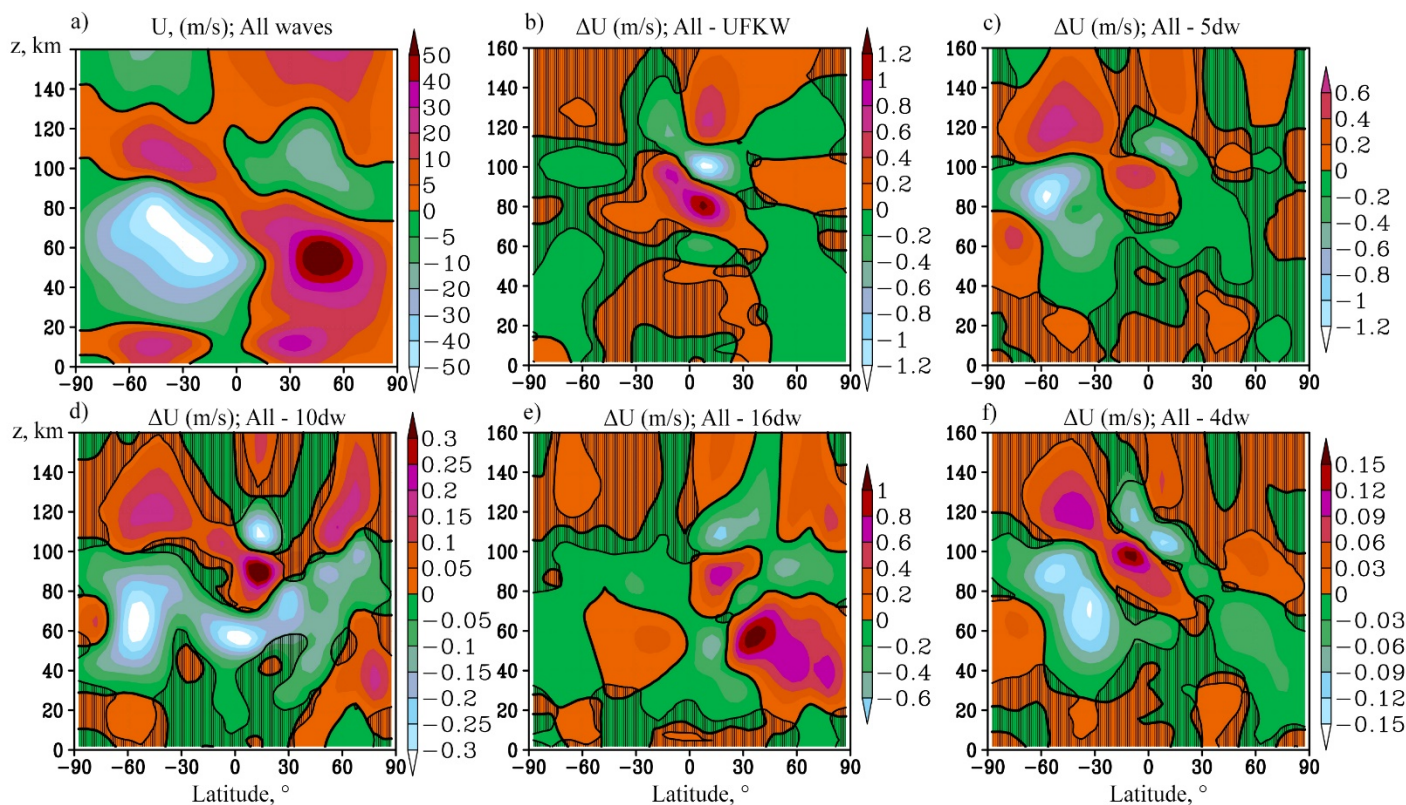
161 The residual meridional circulation (RMC) was calculated to analyze the changes in atmospheric circulation caused
162 by various PWs for each MUAM simulation scenario presented in Table 1, with all PW sources turned on for comparisons
163 with model runs at turned-off sources of particular wave modes. Fig. 2 shows the RMC components and temperature
164 averaged over January-February for model calculation No. 1 (all PW sources included) and differences in these fields due to
165 turning off each of analysed PW mode. Respective zonal-mean zonal wind increments are shown in Fig. 3. Simulated zonal-
166 mean wind (Fig. 3a) and temperature (Fig. 2a) correlate with those obtained with the empirical models HWM-14 (Drob et
167 al., 2015) and NRLMSIS 2.0 (Emmert et al., 2020), also with a semiempirical wind model by Jacobi et al. (2009) and with
168 the MERRA-2 reanalysis data.



169
170 **Figure 2.** a) RMC components (arrows, m/s, vertical component multiplied by 200) and mean zonal temperature components
171 (colours, K) for January-February with all PW sources turned on; b-f) increments in RMC and temperature due to switching off



172 sources of PW: UFKW, 5-, 10-, 16- and 4-day waves, respectively. Shaded areas show insignificant temperature and/or RMC
173 increments at 95%.



174
175 **Figure 3. a) zonal wind components (colours, m/s) for January-February with all PW sources turned on; b-f) increments in zonal**
176 **wind due to switching off sources of PW: UFKW, 5-, 10-, 16- and 4-day waves. Shaded areas show insignificant wind increments at**
177 **95%.**

178 Fig. 2 and 3 show relatively small influence of turning off each individual PW to the zonal-mean temperature and
179 zonal wind. The main impacts are usually localized in the regions of maximum PW amplitudes. The greatest contribution to
180 the circulation change is made by 5-day PW. The main differences in Fig. 2c occur in the southern lower thermosphere,
181 which correspond to a RMC strengthening in a layer between 80 and 120 km after switching on 5-d PW tropospheric source.
182 The acceleration of zonal wind (eastward above 100 km, and westward below) is observed in the same region in Fig. 3c.
183 This effect is primarily explained by the convergence of the Elissen-Palm flux (EP) in this region. The acceleration of the
184 RMC there leads to the lifting up of a warmer air and warming of the atmospheric layer between 60 and 90 km, as well as to
185 the acceleration of air transport from the coldest region of the atmosphere (about 90 km, at latitudes from the South Pole to
186 60° N), which leads to the cooling of the atmosphere above this layer. In addition, in the circumpolar southern stratosphere,
187 at a level of about 60 km, there is deceleration of the zonal wind, which, on the contrary, is associated with the EP flux

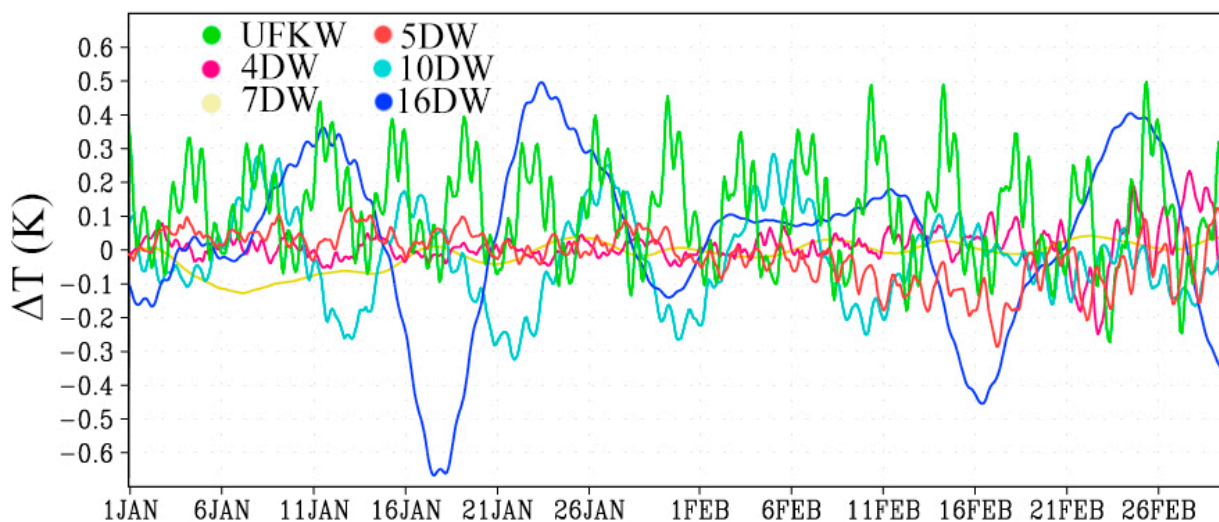


188 divergence.

189 The maximum UFKW amplitude is located at 100 km in the equatorial region (see Fig. 1b). Then the wave
190 propagates higher, gradually attenuating. Its contribution to the circulation flows changes is also maximized in this region
191 and exerted mainly in the strengthening of the zonal wind (Fig. 3b) and the RMC (Fig. 2b). Similar to 5-day PW, the
192 circulation fluxes increments can reach up to 5%. The UFKW impact in the 100-120 km layer leads to cooling in the
193 Northern hemisphere caused by a slowdown in meridional transport and additional updrafts causing adiabatic cooling.

194 16-day wave, as shown above (Fig. 1c), has a maximum in the stratosphere of the Northern hemisphere, and its
195 contribution to atmospheric circulation is observed in this region. Figure 2d shows that introduction of 16-day wave leads to
196 cooling of the layer below 50 km and heating of the overlying layer. The temperature changes here are explained by the
197 change in the RMC components: in particular, the acceleration and weakening of the RMC descending branch contributes to
198 adiabatic heating and cooling, respectively. This is accompanied by acceleration of the zonal wind (Fig. 3e), directed in this
199 region to the east (Fig. 3a).

200 10- and 4-day PW make a smaller contribution to the dynamic and thermal regime of the atmosphere. Specifically,
201 the structure of the 10-day wave in the middle atmosphere is similar to the structure of the 16-day one: the amplitude
202 maximum is observed in the northern stratosphere, but due to the higher phase velocity, its waveguide in the southern middle
203 atmosphere is wider. Propagating in the Southern hemisphere, it contributes to the zonal wind acceleration up to heights of
204 140 km (Fig. 3d) and to the respective temperature changes. A faster 7-day wave, like 5-day wave, is able to propagate along
205 waveguides in both hemispheres. Generally, the 10- and 7-day PW contributions cause the same effects as the 5-day one
206 described above, although they are much weaker in this region.



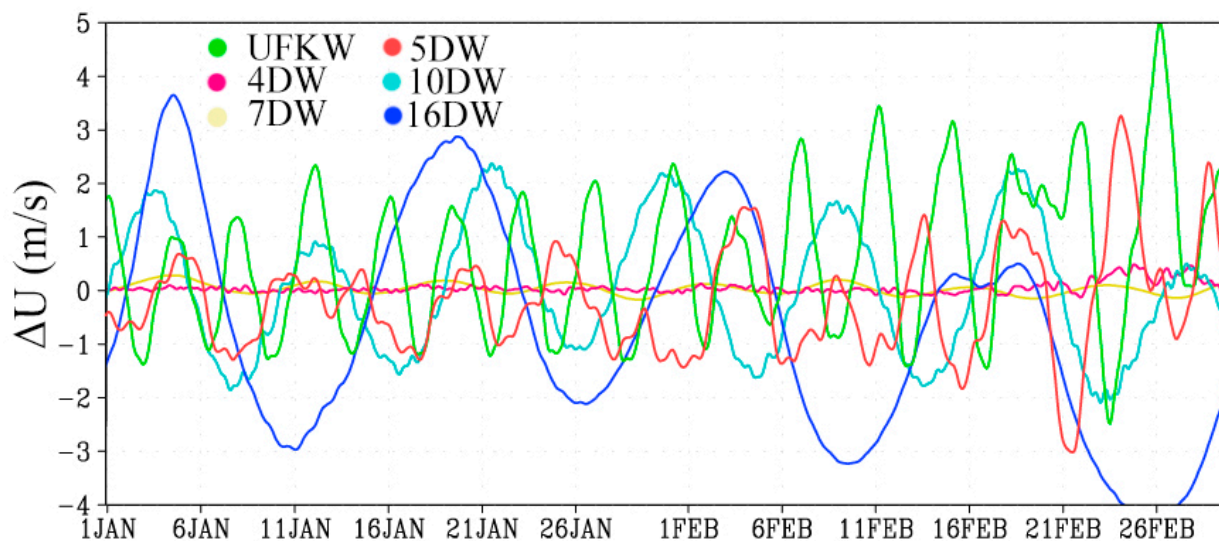
207
208 **Figure 4.** Time series of mean zonal temperature variations due to the inclusion of tropospheric sources of various PW in the
209 regions of their maximum amplitudes in the MUAM.



210 The relatively weak increments, examined in Fig. 2 and 3, require an assessment of statistical significance. Such an
211 assessment was carried out using the Student's paired t-test applied to 45312 pairs of samples in each of the latitude-altitude
212 grid node (64 longitude points \times 708 time points for January-February with a 2-hour model output). Statistically
213 insignificant increments at the 95% significance level are marked with shading. In Fig. 4 shading indicates statistically
214 insignificant data on either temperature or RMC.

215 For a more detailed analysis of the PW effects on atmospheric circulation, the time series of zonal-mean
216 temperature and zonal wind variations due to the considered PW effects were observed – Fig. 4 and 5, respectively. Latitudes
217 and heights corresponding to the maxima of the PW amplitudes were selected: the equator, 100 km is for the UFKW; 5-day
218 wave is considered at 50° S and 105 km; 7-, 10- and 16-day waves: 50° N and 55 km; 4-day wave: 45° S and 105 km.

219



220

221 **Figure 5. Time series of zonal wind variations due to the inclusion of tropospheric sources of various PW in the regions of their**
222 **maximum amplitudes in the MUAM.**

223 In all cases, especially for the zonal wind (Fig. 5), the wave structure of increments with a period corresponding to
224 the period of the considered PW is observed. In particular, wind changes, which significantly exceed the averaged data for
225 January and February (presented in Fig. 3) can be seen in this figure. Specifically, the inclusion of 16-day wave and the
226 UFKW can cause the wind speed changes up to 4 m/s, and up to 5 m/s, respectively. PWs with zonal number 2 (4- and 7-
227 day) make much smaller changes to the zonal flow, while, the weakening of the zonal flow is accompanied by the increase
228 of these waves, as well as the 5-day wave and the UFKW by the end of February. Temperature variations in Fig. 4 have a
229 more complex structure since temperature variations are affected not only by pressure fluctuations, but also by meridional
230 circulation fluctuations.



231 5 Conclusion and summary

232 A number of model simulation have been carried out for January-February, using a 3-dimensional nonlinear
233 mechanistic numerical model of the general circulation of the middle and upper atmosphere MUAM, to estimate the
234 sensitivity of the atmosphere dynamic and thermal regime to the various planetary waves impact. The MUAM model allows
235 to include selectively sources of various PW modes, which gives the opportunity to deeper study the contribution of each
236 PW to the atmospheric circulation structure. Moreover, for a more detailed diagnostics of the PW effect on the mean flow,
237 the transformed Eulerian mean approach was used, implying the calculation of the residual mean meridional circulation,
238 which is a superposition of eddy and advective mean transport.

239 The amplitudes of the simulated PWs are consistent with the ground-based, satellite observations data, as well as
240 with the reanalysis and assimilation of meteorological data. The obtained increments of hydrometeorological parameters are
241 maximal, as a rule, in the regions of maximum amplitudes of the considered PWs. In particular, the inclusion of 5-day PW
242 and an UFKW can transform the speed of the background wind and the component of the residual meridional circulation up
243 to 5%. In turn, changes in the meridional circulation, especially its vertical component, as well as a variation of wave activity
244 fluxes, can cause variations in the background temperature of more than 1 K.

245 The effect of 16-day PW generation by an internal atmospheric source in the southern lower thermosphere,
246 independent of the tropospheric PW sources specified in the model, was found. Most probably, the point is that 4-day PW
247 with a wave number 2 interacts nonlinearly with a 5-day PW with a wave number 1 causing a secondary wave excitation.
248 Such mechanism is described, e.g., by Pogoreltsev (2001): when two waves having frequencies ω and zonal numbers m
249 interact, a new (secondary) wave arises, in which the frequency and wave number are the sum or difference of the
250 corresponding values of the primary waves. However, additional calculations are required to confirm this theory.

251 In addition, it should also be noted that for proper modelling of large-scale atmospheric dynamics, all models of the
252 general atmospheric circulation should be tested for the ability to reproduce the global resonant properties of the atmosphere
253 (the so-called atmospheric normal modes). This possibility has been repeatedly described in MUAM (e.g., Pogoreltsev,
254 2007, Koval et al., 2021), which underlines the reliability of the results obtained.

255
256 **Author Contributions:** All authors have made valuable contributions in writing and editing of the manuscript, data
257 analysis and visualization of the results. A.V.K.: conceptualization, RMC calculation, writing the final version of the
258 manuscript; T.O.N., M.A.M.: numerical modelling; T.S.E. and K.A.D.: statistical processing; G.N.M.: consulting, English
259 editing; E.V.R.: consulting, reanalysis data processing. All authors have read and agreed to the published version of the
260 manuscript.

261
262 **Acknowledgements.** Calculations and interpretation of the residual mean circulation, statistical analysis are
263 supported by the Russian Science Foundation (grant # 20-77-10006). MUAM adjustment, performing numerical simulations



264 of the atmospheric global circulation and calculation of PW structures are supported by the Ministry of Science and Higher
265 Education of the Russian Federation (agreement 075-15-2021-583). All data sets presented in the paper computer codes can
266 be obtained from the corresponding author upon request. All figures in this study are made using Grid Analysis and Display
267 System (GrADS), which is a free software developed thanks to the NASA Advanced Information Systems Research
268 Program. The MERRA-2 dataset can be obtained from https://disc.gsfc.nasa.gov/datasets/M2I6NVANA_5.12.4/summary.

269 **References:**

- 270 Andrews, D. G. and McIntyre, M. E.: Planetary waves in horizontal and vertical shear: The generalized Eliassen-Palm
271 relation and the mean zonal acceleration, *J. Atmos. Sci.*, 33, 2031–2048, [https://doi.org/10.1175/1520-0469\(1976\)033<2031:PWIHAV>2.0.CO;2](https://doi.org/10.1175/1520-0469(1976)033<2031:PWIHAV>2.0.CO;2), 1976.
- 272 Butchart, N.: The Brewer-Dobson circulation, *Rev. Geophys.*, 52, 157–184, <https://doi.org/10.1002/2013RG000448>, 2014.
- 273 Chang, L. C., Yue, L., Wang, W., Wu, Q., and Meier, R. R.: Quasi two day wave-related variability in the background
274 dynamics and composition of the mesosphere/thermosphere and the ionosphere, *Journal of Geophysical Research: Space*
275 *Physics.*, 119, 6, 4786–4804, 2014.
- 276 Charney, J. G. and Drazin, P. G.: Propagation of planetary-scale disturbances from the lower into the upper atmosphere, *J.*
277 *Geophys. Res.*, 66, 83–109, 1961.
- 278 Clark, R., Burrage, M., Franke, S., Manson, A., Meek, C., Mitchell, N., and Muller, H.: Observations of 7-d planetary waves
279 with MLT radars and the UARS-HRDI instrument, *Journal of Atmospheric and Solar-Terrestrial Physics*, 64 ,8/11, 1217–
280 1228, 2002.
- 281 Day, K. A., Hibbins, R. E., and Mitchell, N. J.: Aura MLS observations of the westward-propagating 16-day planetary wave
282 in the stratosphere, mesosphere and lower thermosphere, *Atmos. Chem. Phys.*, 11, 4149–4161, <https://doi.org/10.5194/acp-11-4149-2011>, 2011.
- 283 Drob, D. P., Emmert, J. T., Meriwether, J. W., Makela, J. J., Doornbos, E., Conde, M., Hernandez, G., Noto, G., Zawdie, K.
284 A., McDonald, S. E., Huba, J. D., and Klenzing, J. H.: An update to the Horizontal Wind Model (HWM): The quiet time
285 thermosphere, *Earth and Space Science*, 2, 301–319, <https://doi.org/10.1002/2014EA000089>, 2015.
- 286 Eliassen A. and Palm E.: On the transfer of energy in stationary mountain waves // *Geophys. Norv.*, 22, 1–23, 1961.
- 287 Emmert, J. T., Drob, D. P., Picone, J. M., Siskind, D. E., Jones, M. Jr., Mlynczak, M. G., et al.: NRLMSIS 2.0: A
288 whole-atmosphere empirical model of temperature and neutral species densities, *Earth and Space Science*, 7,
289 e2020EA001321, <https://doi.org/10.1029/2020EA001321>, 2020.
- 290 Ermakova T. S., Aniskina, O. G., Statnaya, I. A., Motsakov, M. A., and Pogoreltsev A. I.: Simulation of the ENSO influence
291 on the extra-tropical middle atmosphere, *Earth, Planets and Space*. 71, 8, <https://doi.org/10.1186/s40623-019-0987-9>, 2019.
- 292 Forbes, J. M. and Zhang, X.: The quasi-6 day wave and its interactions with solar tides, *Journal of Geophysical Research:*
293 *Space Physics*, 122, 4764–4776, <https://doi.org/10.1002/2017JA023954>, 2017.



- 296 Forbes, J. M., Zhang, X., and Maute, A.: Planetary wave (PW) generation in the thermosphere driven by the PW-modulated
297 tidal spectrum, *Journal of Geophysical Research: Space Physics*, 125, e2019JA027704,
298 <https://doi.org/10.1029/2019JA027704>, 2020.
- 299 Forbes, J. M., Zhang, X., Maute, A., and Hagan, M. E.: Zonally symmetric oscillations of the thermosphere at planetary
300 wave periods, *Journal of Geophysical Research: Space Physics*, 123, 4110–4128, <https://doi.org/10.1002/2018JA025258>,
301 2018.
- 302 Gavrilov, N. M., Koval, A. V., Pogoreltsev, A. I., and Savenkova, E. N.: Simulating planetary wave propagation to the upper
303 atmosphere during stratospheric warming events at different mountain wave scenarios, *Advances in Space Research*. 61, 7,
304 1819–1836, <https://doi.org/10.1016/j.asr.2017.08.022>, 2018.
- 305 Gelaro, R., McCarty, W., Suárez, Max J., Todling, R., Molod, A., Takacs, L., Randles, C., Darmenov, A., Bosilovich, M.
306 G., Reichle, R., Wargan, K., Coy, L., Cullather, R., Draper, C., Akella, S., Buchard, V., Conaty, A., da Silva, A., Wei Gu,
307 Gi-Kong Kim, Koster, R., Lucchesi, R., Merkova, D., Nielsen, J. E., Partyka, G., Pawson, S., Putman, W., Rienecker, M.,
308 Schubert, S. D., Sienkiewicz, M. and Zhao, B. The Modern-Era Retrospective Analysis for Research and Applications,
309 Version 2 (MERRA-2), *J. Clim.*, Volume 30, 13, 5419–5454, <https://doi.org/10.1175/JCLI-D-16-0758.1>, 2017.
- 310 Haynes, P. H., McIntyre, M. E., Shepherd, T. G., Marks, C. J., and Shine, K. P. On the “downward control” of extratropical
311 diabatic circulations by eddy-induced mean zonal forces, *J. Atmos. Sci.* 48, 4, 651–678, 1991.
- 312 He, M., Chau, J. L., Forbes, J. M., Thorsen, D., Li, G., Siddiqui, T. A., et al.: Quasi-10-day wave and semidiurnal tide
313 nonlinear interactions during the Southern Hemispheric SSW 2019 observed in the Northern Hemispheric mesosphere,
314 *Geophysical Research Letters*, 47, e2020GL091453, <https://doi.org/10.1029/2020GL091453>, 2020.
- 315 Holton, J. R.: The dynamic meteorology of the stratosphere and mesosphere, *Meteorol. Monogr.* 15, 37, 218 p., 1975.
- 316 Holton, J. R., Haynes, P. H., McIntyre, M. E., Douglas, A. R., Rood, R. B., and Pfister, L.: Stratosphere-troposphere
317 exchange, *Rev. Geophys.* 33, 403–439, 1995.
- 318 Holton, J. R. and Tan, H.: The influence of the equatorial quasibiennial oscillation on the global circulation at 50 mb, *J.*
319 *Atmos. Sci.* 37, 2200–2208, 1980.
- 320 Huang, Y., Zhang, S., Li, C., Li, H., Huang, K., and Huang, C.: Annual and interannual variations in global 6.5 DWS from
321 20 to 110 km during 2002–2016 observed by TIMED/SABER, *Journal of Geophysical Research: Space Physics*, 122, 8985–
322 9002, <https://doi.org/10.1002/2017JA023886>, 2017.
- 323 Jacobi, Ch., Fröhlich, K., and Portnyagin, Y. Semi-empirical model of middle atmosphere wind from the ground to the lower
324 thermosphere, *Adv. Space Res.* 43, 239–246, 2009.
- 325 Jiang, G.-y., Xu, J., Xiong, J., Ma, R., Ning, B., Murayama, Y., et al.: A case study of the mesospheric 6.5-day wave
326 observed by radar systems, *Journal of Geophysical Research*, 113, D16111, <https://doi.org/10.1029/2008JD009907>, 2008.
- 327 Koval, A. V., Gavrilov, N. M., Pogoreltsev, A. I., and Kandieva, K. K.: Dynamical impacts of stratospheric QBO on the
328 global circulation up to the lower thermosphere, *Journal of Geophysical Research: Atmospheres*, 127, e2021JD036095.
329 <https://doi.org/10.1029/2021JD036095>, 2022.



- 330 Koval, A. V., Gavrilov, N. M., Pogoreltsev, A. I., and Shevchuk, N. O.: Influence of solar activity on penetration of traveling
331 planetary-scale waves from the troposphere into the thermosphere, *Journal of Geophysical Research: Space Physics*, 123, 8,
332 6888–6903, <https://doi.org/10.1029/2018JA025680>, 2018a.
- 333 Koval, A. V., Gavrilov, N. M., Pogoreltsev, A. I., and Savenkova, E. N.: Comparisons of planetary wave propagation to the
334 upper atmosphere during stratospheric warming events at different QBO phases, *Journal of Atmospheric and Solar-
335 Terrestrial Physics*, 171, 201–209, <https://doi.org/10.1016/j.jastp.2017.04.013>, 2018b.
- 336 Liu, H. L., Talaat, E. R., Roble, R. G., Lieberman, R. S., Riggins, D. M., and Yee, J. H.: The 6.5-day wave and its seasonal
337 variability in the middle and upper atmosphere, *Journal of Geophysical Research-Atmospheres*, 109, D21,
338 <https://doi.org/10.1029/2004jd004795>, 2004.
- 339 Longuet-Higgins, M. S.: The eigenfunctions of Laplace's tidal equation over a sphere. *Philos. T. R. Soc. Lond.* 262: 511–
340 607, 1968.
- 341 Medvedeva, I. V., Semenov, A. I., Pogoreltsev, A. I., and Tatarnikov, A. V.: Influence of sudden stratospheric warming on
342 the mesosphere/lower thermosphere from the hydroxyl emission observations and numerical simulations, *Journal of
343 Atmospheric and Solar-Terrestrial Physics*, 187, 22–32, <https://doi.org/10.1016/j.jastp.2019.02.005>, 2019.
- 344 Merzlyakov, E., Solovjova, T., and Yudakov, A.: The interannual variability of a 5–7 day wave in the middle atmosphere in
345 autumn from era product data, aura MLS data, and meteor wind data, *Journal of Atmospheric and Solar-Terrestrial Physics*,
346 102, 281–289, 2013.
- 347 Nath, D., Chen, W., Zelin, C., Pogoreltsev, A. I., and Wei, K. Dynamics of 2013 Sudden Stratospheric Warming event and
348 its impact on cold weather over Eurasia: Role of planetary wave reflection, *Sci. Rep.* 6, 24174,
349 <https://doi.org/10.1038/srep24174>, 2016.
- 350 Newman, P. A., Oman, L. D., Douglass, A. R., Fleming, E. L., Frith, S. M., Hurwitz, M. M., Kawa, S. R., Jackman, C. H.,
351 Krotkov, N. A., Nash, E. R., Nielsen, J. E., Pawson, S., Stolarski, R. S., and Velders, G. J. M.: What would have happened to
352 the ozone layer if chlorofluorocarbons (CFCs) had not been regulated? *Atmos. Chem. Phys.*, 9, 2113–2128,
353 <https://doi.org/10.5194/acp-9-2113-2009>, 2009.
- 354 Pancheva, D., Mukhtarov, P., Andonov, B., and Forbes, J. M.: Global distribution and climatological features of the 5-6-day
355 planetary waves seen in the SABER/TIMED temperatures (2002-2007). *J. Atmos. Solar-Terr. Phys.*, 72, 1, 26–37, 2010.
- 356 Pancheva, D., Mukhtarov, P., Andonov, B., Mitchell, N. J., and Forbes, J. M. Planetary waves observed by TIMED/SABER
357 in coupling the stratosphere- mesosphere-lower thermosphere during the winter of 2003/2004: part 2—altitude and latitude
358 planetary wave structure, *J. Atmos. Solar-Terr. Phys.* 71, 1, 75–87, <https://doi.org/10.1016/j.jastp.2008.09.027>, 2009.
- 359 Pancheva, D., Mukhtarov, P., Mitchell, N. J., Merzlyakov, E., Smith, A. K., Andonov, B., Singer, W., Hocking, W., Meek,
360 C., Manson, A., and Murayama, Y. Planetary waves in coupling the stratosphere and mesosphere during the major
361 stratospheric warming in 2003/2004, *J. Geophys. Res.* 113, D12, D12105, <https://doi.org/10.1029/2007JD009011>, 2008.



- 362 Pancheva, D., Mukhtarov, P., and Siskind, D. E.: The quasi-6-day waves in NOGAPS-ALPHA forecast model and their
363 climatology in MLS/Aura measurements (2005–2014), *Journal of Atmospheric and Solar-Terrestrial Physics*, 181, 19–37,
364 2018.
- 365 Pedatella, N. M. and Forbes, J. M.: Modulation of the equatorial F-region by the quasi-16-day planetary wave, *Geophys.*
366 *Res. Lett.*, 36, L09105, <https://doi.org/10.1029/2009GL037809>, 2009.
- 367 Pogoreltsev, A. I. (2007). Generation of normal atmospheric modes by stratospheric vacillations. *Izvestiya Atmos. Ocean.*
368 *Phys.* 43(4), 423–435.
- 369 Pogoreltsev, A. I. Numerical simulation of secondary planetary waves arising from the nonlinear interaction of the normal
370 atmospheric modes. *Phys. Chem. Earth (Part C)*. 26(6), 395–403 (2001).
- 371 Pogoreltsev, A. I.: Simulation of planetary waves and their influence on the zonally averaged circulation in the middle
372 atmosphere, *Earth, Planets Space*. 51, 7/8, 773–784, 1999.
- 373 Pogoreltsev, A.I., Vlasov, A.A., Froehlich, K., and Jacobi, Ch.: Planetary waves in coupling the lower and upper
374 atmosphere, *J. Atmos. Solar-Terr. Phys.* 69, 2083–2101, <https://doi.org/10.1016/j.jastp.2007.05.014>, 2007.
- 375 Qin, Y., Gu, S.-Y., and Dou, X.: A new mechanism for the generation of quasi-6-day and quasi-10-day waves during the
376 2019 Antarctic sudden stratospheric warming, *Journal of Geophysical Research: Atmospheres*, 126, e2021JD035568,
377 <https://doi.org/10.1029/2021JD035568>, 2021.
- 378 Sassi, F., Garcia, R., and Hoppel, K.: Large-scale Rossby normal modes during some recent Northern Hemisphere winters,
379 *Journal of the Atmospheric Sciences*, 69, 3, 820–839, 2012.
- 380 Schoeberl, M.: Stratospheric warmings – observations and theory, *Rev. Geophys.* 16, 521–538.
381 <https://doi.org/10.1029/RG016i004p00521>, 1978.
- 382 Swarztrauber, P. N. and Kasahara, A.: The vector harmonic analysis of Laplace's tidal equations, *SIAM J. Sci. Stat. Comp.* 6,
383 464–491, 1985.
- 384 Wang, J. C., Chang, L. C., Yue, J., Wang, W., and Siskind, D. E.: The quasi 2 day wave response in TIME-GCM nudged
385 with NOGAPS-ALPHA, *Journal of Geophysical Research: Space Physics*, 122, 5, 5709–5732, 2017.
- 386 Yamazaki, Y., Matthias, V., and Miyoshi, Y.: Quasi-4-day wave: Atmospheric manifestation of the first symmetric Rossby
387 normal mode of zonal wavenumber 2, *Journal of Geophysical Research: Atmospheres*, 126, e2021JD034855,
388 <https://doi.org/10.1029/2021JD034855>, 2021.
- 389